Resonant Raman scattering in self-assembled GaN/AlN quantum dots

N. Garro, A. Cros, J. M. Llorens, A. García-Cristóbal, and A. Cantarero
Institut de Ciència dels Materials, Universitat de València, E-46071 València, Spain

N. Gogneau, E. Sarigiannidou, E. Monroy, and B. Daudin
CEA-CNRS group "Nanophysique et Semiconducteurs," Département de la Recherche Fondamentale sur la Matière Condensée, CEA-Grenoble, 17 rue des Martyrs, 38054-Grenoble Cedex 9, France
(Received 5 May 2006; published 2 August 2006)

Self-assembled GaN/AlN quantum dots have been investigated by means of Raman scattering. A resonant enhancement of the Raman peaks has been observed when the excitation is tuned above the GaN band-gap energy. The polar mode nature, either quasiconfined or interfacial, has been assigned after comparing with the polar optical modes of spheroidal dots calculated within the framework of the anisotropic dielectric continuum model. The built-in strain of the GaN dots induced a substantial blueshift of the nonpolar E_{2H} Raman mode frequency. A theoretical model that analyzes the three-dimensional strain distribution in the quantum dots has been employed for estimating the strain contribution to the frequency shifts of both nonpolar and polar optical modes.

DOI: 10.1103/PhysRevB.74.075305 PACS number(s): 78.67.Hc, 78.30.Fs, 63.22.+m

I. INTRODUCTION

The demonstration of the Stranski-Krastanow growth mode when GaN is deposited on AlN by molecular beam epitaxy[1] pointed out a promising new generation of optoelectronic devices based on GaN quantum dots (QD's). In particular, these systems could be a good material support for solid-state quantum computation by exploiting the existence of a strong built-in electric field to generate entangled few-exciton states.[2] Such an electric field, which can reach values as high as 7 MV/cm,[3] mainly originates in the difference in the electrostatic polarization between the dot and the barrier materials. In addition to the spontaneous polarization characteristic of group-III nitrides,[4] piezoelectric fields induced by strain also play an important role due to the strength of the piezoelectric constants of these materials, which are more than one order of magnitude larger than those of other III-V semiconductors. Therefore, knowing the strain distribution in dots and barriers is essential for the good understanding of the optical and electronic properties of self-assembled GaN/AlN QD's.

Raman scattering spectroscopy is a suitable technique to probe the strain field in semiconductor heterostructures.[5] Significant strain-induced phonon frequency shifts have been observed in the Raman spectra of self-assembled GaN/AlN QD's. Although most Raman studies have been interpreted assuming the so-called biaxial strain approximation (i.e., $\varepsilon_{xx}=\varepsilon_{yy}$ and $\varepsilon_{zz}=-2C_{13}/C_{33}\varepsilon_{xx}$, with z parallel to the wurtzite c axis),[6–8] a recent detailed work has evidenced the nonbiaxial nature of the strain field in GaN/AlN QD's and the need of a careful theoretical analysis of the Raman spectra.[9] In addition to the effects induced by strain, Raman scattering spectroscopy is also sensitive to the presence of interfaces. Polar optical modes of quantum wells and superlattices are substantially different from those of bulk materials and can be either confined in one of the materials or localized at the interfaces. In the case of GaN/AlN systems, confined phonons penetrate into the barrier material due to the anisotropy of the wurtzite structure.[10,11] Furthermore, these quasi-confined modes are dispersive and, when the angle between the phonon wave vector and the c axis is different from 0 or $\pi/2$, have a mixed symmetry, becoming quasi-TO or -LO modes.[11] The theoretical study of polar optical phonons in wurtzite QD's has been tackled recently within the dielectric-continuum model,[12,13] and frequencies significantly different from those of the bulk material have been predicted for spheroidal dots.

In the present work we investigate the Raman scattering spectra of GaN/AlN QD multilayer systems. First, we present the Raman spectra for different polarization configurations and excitation energies. Confinement effects in the spectra of polar optical modes are discussed qualitatively by comparing with the calculated frequencies of oblate spheroidal dots. The strain-induced frequency shifts of nonpolar Raman modes are also analyzed with the aid of a theoretical model for the elastic strain relaxation inside QD's of realistic shape. Finally, both theoretical results are combined in order to estimate the frequencies of polar optical modes.

II. SAMPLE DESCRIPTION AND EXPERIMENTAL SETUP

Two samples have been investigated in this study. Sample $S1$ consists of a stack of 50 periods of GaN QD's separated by 8.6-nm-thick AlN spacers, grown by plasma-assisted molecular beam epitaxy at a growth temperature of 750 °C. The substrate is a 1-μm-thick AlN layer grown by metalorganic chemical vapor deposition on sapphire.[14] The QD multilayer was grown on a 100 nm AlN buffer layer and capped with a 100-nm-thick AlN layer. Sample $S2$ contained 200 periods of GaN QD's with 8 nm AlN barriers and was grown on a 6H-SiC (0001) substrate kept at 730 °C during the growth. A very thin AlN buffer layer, of 10 nm, was grown prior to the deposition of the dots and no capping was added after the last QD period. In both cases, the growth procedure was a modification of the Stranski-Krastanow mode[15] where each QD period formed after the deposition of a few monolayers of metastable two-dimensional GaN in Ga-rich conditions.

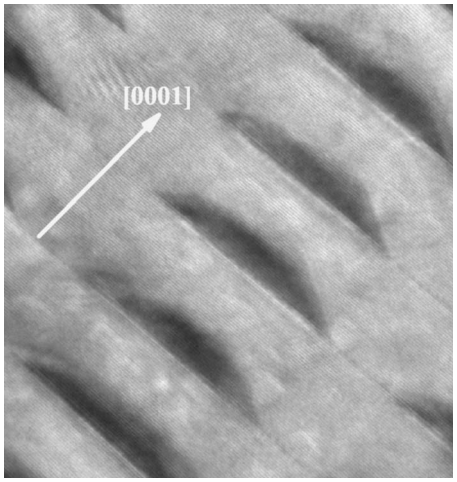

FIG. 1. HRTEM image of a few GaN/AlN QD layers of sample *S*1.

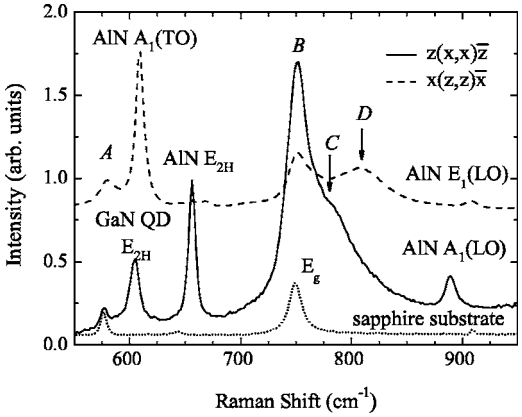

FIG. 2. Raman spectra of sample *S*1 obtained under 3.72 eV excitation for two polarization configurations. The z direction coincides with the c axis of the wurtzite structure. The dotted line corresponds to the Raman spectrum of a sapphire substrate in the $z(x,x)\bar{z}$ scattering configuration.

The Ga surfactant effect inhibits the formation of GaN islands. The rearrangement of the two-dimensional (2D) GaN layer into 3D dots is induced by a growth interruption of 2 min. Under these growth conditions, the expected QD densities are 2×10^{11} and 5×10^{10} cm^{-2} for samples *S*1 and *S*2, respectively.[15]

High-resolution transmission electron microscopy (HRTEM) of sample *S*1 (see Fig. 1) shows that the buried QD's are truncated pyramids with 32° facet angles standing on a two monolayer GaN wetting layer (WL). The average diameter and height of the dots are 20.5 ± 0.5 and 4.3 ± 0.5 nm, respectively. The observed vertical alignment of the QD's has been attributed to the propagation of the strain field induced by the buried dots through the AlN barrier.[17] Minima of the elastic energy density are predicted at the surface of the spacer right on top of each buried dot which act as nucleation centers.[16] The average dot height (3.8 ± 1.0 nm) and diameter (50 ± 1 nm) in sample *S*2 were determined by means of atomic force microscopy.[18]

Raman scattering measurements are carried out with a Jobin-Yvon T64000 spectrometer equipped with a confocal microscope and a nitrogen-cooled charge-coupled device detector. Several lines of an argon laser comprising a wide energy range (from 2.2 to 4.5 eV) are used for excitation. The diameter of the laser spot is 1 and 4 μm for visible and ultraviolet laser excitation, respectively. All measurements were performed at room temperature.

III. EXPERIMENTAL RESULTS

The Raman spectra of sample *S*1 recorded in backscattering geometry under 3.72 eV (333 nm) excitation are shown in Fig. 2 for two different polarization configurations. The lowest spectrum corresponds to the sapphire substrate in the $z(x,x)\bar{z}$ scattering configuration. The excitation energy is below the WL emission (at ~4.6 eV),[19] much below the AlN band gap (at 6.2 eV), and above the QD emission (typically around 2.5–3.2 eV). Thus, the excitation energy is resonant with the absorption of the QD excited states. Several GaN- and AlN-like Raman peaks are observed in Fig. 2. Given the size and density of the dots, we estimate that more than 85% of the GaN in the sample corresponds to the QD's. Thus, the GaN-related peaks are attributed to the QD's, neglecting the contribution of the 2D WL. In Fig. 2, the zone center phonons of AlN appear at their bulk frequencies. On the other hand, the peaks ascribed to the GaN QD's are clearly blueshifted with respect to GaN bulk frequencies (summarized in Table I). This is the case of the peak centered at 604 ± 1 cm^{-1}, which can be assigned to the E_{2H} mode of the QD's, as done in a previous work.[6] The peak centered at 582 ± 1 cm^{-1} (preliminarily labeled as mode *A*) appearing in $x(z,z)\bar{x}$ polarization configuration follows A_1(TO) selection rules. The assignment of this mode as a quasiconfined TO or an interface mode will be discussed further on. For similar reasons, the peak centered at 751 ± 1 cm^{-1} (mode *B*) could be attributed to a quasiconfined LO mode of the dots. Notice that although this mode coincides in frequency with an E_g mode of the sapphire substrate, allowed in the $z(x,x)\bar{z}$ scattering configuration, the intensity of the latter is considerably weaker than the signal from the GaN QD's under resonant excitation (see Fig. 2) so that the contribution of the substrate can be effectively neglected. Two additional broad peaks centered at 780 ± 2 cm^{-1} (mode *C*) and 802 ± 2 cm^{-1} (mode *D*) appear at the high-energy side of mode *B* in Fig. 2. To the best of our knowledge, these modes have not been reported in the literature before and, therefore, their origin needs to be discussed carefully. One possible explanation could be that they are the quasi-LO modes of an $Al_xGa_{1-x}N$ alloy that forms due to interdiffusion between the dots and the barriers.

TABLE I. Optical dielectric constants $\epsilon_\perp(\infty)=\epsilon_z(\infty)$ and frequencies in cm^{-1} of the bulk phonons of GaN (Ref. 20) and AlN (Ref. 21).

Material	$\epsilon(\infty)$	E_{2H}	A_1(TO)	E_1(TO)	A_1(LO)	E_1(LO)
GaN	5.29	568	531	558.8	734	741
AlN	4.68	655.5	609	669	891	912

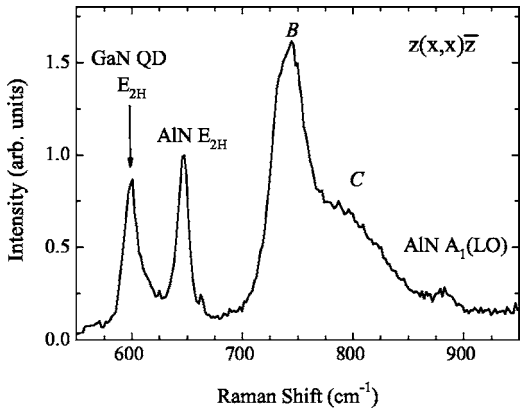

FIG. 3. Raman spectrum of sample $S2$ obtained under 4.51 eV excitation for $z(x,x)\bar{z}$ scattering configuration.

This can be ruled out at the sight of the HRTEM image (see Fig. 1) which, in agreement with energy-filtered TEM experiments[17] carried out on similar samples, shows no signs of Al-Ga intermixing. Alternatively, these Raman peaks could also be assigned to interface confined modes, as will be discussed in Sec. IV.

Figure 3 shows the Raman spectrum of sample $S2$ recorded in $z(x,x)\bar{z}$ polarization configuration under 4.51 eV (275 nm) excitation. No Raman signal from the 6H-SiC substrate can be observed in the spectrum indicating that the excitation is effectively absorbed by the QD's. The E_{2H} nonpolar phonons appear at 597 ± 1 cm^{-1} and 645 ± 1 cm^{-1} for the GaN dot and the AlN barrier, respectively, and are shifted with respect to their bulk values. In the same manner as in sample $S1$, two intense peaks, attributed to modes B and C, are clearly observed in the range comprised between 750 and 800 cm^{-1}. In particular, mode B is centered at 741 ± 1 cm^{-1} and mode C at 799 ± 3 cm^{-1}. The slight differences in the QD Raman frequencies between samples $S1$ and $S2$ are due to the fact that they are grown on different substrates and contain a rather different amount of AlN in the buffer and capping layers. The shift of the AlN E_{2H} mode in sample $S2$ can be explained by attending to the higher number of QD layers, the thinner AlN buffer layer, and the lack of an AlN capping layer. Strain-induced frequency shifts on the E_{2H} nonpolar phonons of sample $S2$ have been studied in previous work.[9] In spite of the minor differences, the measurements carried out on sample $S2$ prove the reproducibility of the results of sample $S1$. Therefore, from now on, our study will be focused on sample $S1$.

In order to get further insight into the origin of the modes here reported, Raman scattering measurements on sample $S1$ have been carried out tuning the excitation energy over a wide range. Raman spectra corresponding to three different excitation energies are depicted in Figs. 4(a) and 4(b) for the same polarization configurations studied in Fig. 2. In order to compare the intensities of the different spectra, these have been normalized to the maximum intensities of two AlN modes. Notice that, within the studied energy range, the AlN matrix is transparent to the laser radiation and therefore no significant variation of the intensity is expected for the AlN Raman modes. On the other hand, there is a clear enhancement of the Raman intensity of the modes B, C, and D when the excitation is tuned above the GaN band-gap energy but is still below the WL absorption edge. An enhancement of modes E_{2H} and A is also observed but to a lesser degree. The maximum absorption of the QD's is expected to be blue-shifted with respect to the emission energy due to the presence of giant internal electric fields. Therefore the observed resonant enhancement of the Raman signal can be attributed to electron-phonon interaction between polar phonons and electronic states localized in the GaN QD's. The experimental results shown in Fig. 4 therefore confirm the polar nature of modes A, B, C, and D. Furthermore, the stronger resonant enhancement of modes B, C, and D is characteristic of Fröhlich electron-phonon interaction[22] and points out the longitudinal character of these modes.

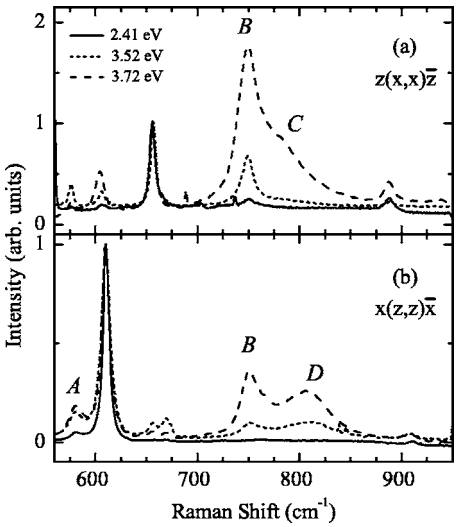

FIG. 4. Raman spectra of sample $S1$ measured for different excitation energies. The spectra are normalized to the maximum intensity of AlN E_{2H} (a), and A_1 (TO) (b) modes.

IV. DISCUSSION

The interpretation of the Raman spectra presented above with a detailed assignment of the observed phonons would require a theoretical model that takes into account the confinement and the strain effects on the phonons of GaN/AlN QD's, as well as the piezoelectric and pyroelectric properties of the two materials. The latter are second-order corrections and introduce minor frequency shifts in comparison with those originated by strain, as shown for the phonons of GaN/AlN quantum wells and superlattices.[23] Hence, we shall neglect the piezoelectric effects and focus on confinement and strain field effects. Even so, a microscopic model for the atomic vibrations of a QD of realistic shape that also includes the inhomogeneous strain distribution in the dot and in the surrounding barrier is not available in the literature yet. Instead, we shall analyze the confinement effects for spheroidal QD's, as this problem has an analytical solution.[13] The strain-induced frequency shifts will be studied separately for QD's of realistic shape. Finally, the results of both theoretical models will be combined in order to discuss the experimental results.

A. Confinement effects on polar optical phonons

While assuming that the atoms of a QD vibrate in the same manner as in a bulk sample can be valid for nonpolar E_2 modes, the presence of interfaces affects the optical polar modes significantly. Within the framework of the anisotropic dielectric continuum model, the electric potential of a polar mode is defined piecewise as $V_k(\mathbf{r})$, with $k=1$ denoting the GaN QD volume and $k=2$ the surrounding AlN matrix. The potential must satisfy Laplace's equation in both regions

$$-\nabla(\hat{\epsilon}_k(\omega)\nabla V_k(\mathbf{r}))=\mathbf{0}, \tag{1}$$

where $\hat{\epsilon}_k(\omega)$ are the bulk dielectric tensors of GaN ($k=1$) and AlN ($k=2$), which, for uniaxial media, adopt the general form

$$\hat{\epsilon}_k(\omega)=\begin{pmatrix}\epsilon_\perp^{(k)}(\omega) & 0 & 0\\ 0 & \epsilon_\perp^{(k)}(\omega) & 0\\ 0 & 0 & \epsilon_z^{(k)}(\omega)\end{pmatrix}. \tag{2}$$

The dielectric functions can be written as

$$\epsilon_\perp^{(k)}(\omega)=\epsilon_\perp^{(k)}(\infty)\frac{\omega^2-(\omega_{E_1,LO}^{(k)})^2}{\omega^2-(\omega_{E_1,TO}^{(k)})^2},$$

$$\epsilon_z^{(k)}(\omega)=\epsilon_z^{(k)}(\infty)\frac{\omega^2-(\omega_{A_1,LO}^{(k)})^2}{\omega^2-(\omega_{A_1,TO}^{(k)})^2}. \tag{3}$$

Besides Eq. (1), continuity of the potential and the normal projection of the displacement vector at the QD surfaces must be satisfied. Thus, for $\mathbf{r}_S\in S$,

$$V_1(\mathbf{r}_S)=V_2(\mathbf{r}_S),$$

$$\mathbf{D}_1(\mathbf{r}_S)\mathbf{n}_S=\mathbf{D}_2(\mathbf{r}_S)\mathbf{n}_S. \tag{4}$$

The solution of Eqs. (1) and (4) for a QD of realistic shape is not analytical and requires numerical calculations[13] out of the scope of the present study. Recently an analytical solution for dots of spheroidal shape has been reported,[13] with a surface given by

$$\frac{x^2+y^2}{R^2}+\frac{z^2}{h^2}=1. \tag{5}$$

The solutions in this case can be written in terms of the associated Legendre functions of the first and second kind, P_l^m and Q_l^m, as

$$V_1(\mathbf{r})=\frac{P_l^m(\xi_1(\mathbf{r}))}{P_l^m(\xi_1(\mathbf{r}_S))}P_l^m(\eta_1(\mathbf{r}))e^{im\phi},$$

$$V_2(\mathbf{r})=\frac{Q_l^m(\xi_2(\mathbf{r}))}{Q_l^m(\xi_2(\mathbf{r}_S))}P_l^m(\eta_2(\mathbf{r}))e^{im\phi}, \tag{6}$$

where (ξ_k,η_k) are the spheroidal coordinates related to the Cartesian coordinates by

$$\sqrt{x^2+y^2}=R\sqrt{\left(\frac{1}{g_k(\omega)}-1\right)(\xi_k^2-1)(1-\eta_k^2)},$$

$$z=h\sqrt{1-g_k(\omega)}\xi_k\eta_k, \tag{7}$$

with

$$g_k(\omega)=\frac{R^2}{h^2}\frac{\epsilon_z^{(k)}(\omega)}{\epsilon_\perp^{(k)}(\omega)}. \tag{8}$$

When the phonon potentials (6) are introduced into the boundary conditions (4), the following secular equation can be deduced:[13]

$$\epsilon_z^{(1)}(\omega)\left(\xi\frac{d\ln P_l^m(\xi)}{d\xi}\right)\Bigg|_{\xi=1/\sqrt{1-g_1(\omega)}}=\epsilon_z^{(2)}(\omega)\left(\xi\frac{d\ln Q_l^m(\xi)}{d\xi}\right)\Bigg|_{\xi=1/\sqrt{1-g_2(\omega)}}. \tag{9}$$

This equation defines the frequencies of the polar optical modes of a wurtzite spheroidal QD embedded in a matrix. It should be pointed out that the solutions of Eq. (9) depend only on the dot aspect ratio h/R. As discussed in Ref. 13, $g_2(\omega)$ is positive for all physical solutions, which are then classified as quasiconfined or interface modes depending on the sign of $g_1(\omega)$. If $g_1(\omega)<0$, then $0<\xi_1<1$ and $P_l^m(\xi_1)$ in Eq. (6) is an oscillatory function. This corresponds to a mode confined in the QD and occurs when $\omega_{A_1,TO}^{(1)}<\omega<\omega_{E_1,TO}^{(1)}$ for TO quasiconfined modes, and when $\omega_{A_1,LO}^{(1)}<\omega<\omega_{E_1,LO}^{(1)}$ for LO quasiconfined modes. On the other hand, when $g_1(\omega)>0$, ξ_1 is larger than 1 or purely imaginary, and $P_l^m(\xi_1)$ reaches its maximum at the dot surface. Thus, these solutions are interface modes and their frequencies are comprised within $\omega_{E_1,TO}^{(1)}<\omega<\omega_{A_1,TO}^{(2)}$ for TO interface modes, $\omega_{E_1,TO}^{(2)}<\omega<\omega_{A_1,LO}^{(1)}$ for mixed modes, and $\omega_{E_1,LO}^{(1)}<\omega<\omega_{A_1,LO}^{(2)}$ for LO modes. Opposite to the case of GaAs/AlAs QD's,[24] interface modes cannot be uniquely associated either with the dot or with the barrier materials.

Equation (9) has been solved for the case of an oblate spheroid GaN dot with AlN barriers (the parameters employed in the calculations are listed in Table I). The solutions corresponding to $m=0$ and $l=1,2,3,4$ are shown in Fig. 5 as a function of the dot aspect ratio h/R. Frequencies of polar optical modes with $m>0$ and $l\geqslant m$ are similar to the $m=0$ results and have not been included in Fig. 5 for clarity. Moreover, the vibrational modes with higher symmetry, i.e., smaller m and l quantum numbers, couple more strongly to photons and are more likely to be observed in the Raman spectra. The calculations show that LO quasiconfined modes exist only for very flat QD's (with aspect ratios below 0.01). On the other hand, there are two TO quasiconfined modes whose frequencies vary slowly with the aspect ratio of the dot. Eight interface modes, four of them LO and the other four TO, appear for most of the studied h/R range. Although interface modes cannot be fully assigned to the dot or the barrier, some modes are closer to AlN or to GaN bulk frequencies, and can be regarded as quasi-AlN or quasi-GaN modes. This is clearly seen for the LO interface modes of flat QD's (small h/R) shown in Fig. 5 where modes with $l=1,3$ are more GaN-like and modes $l=2,4$ are quasi-AlN. The interface mode frequencies depend strongly on the QD

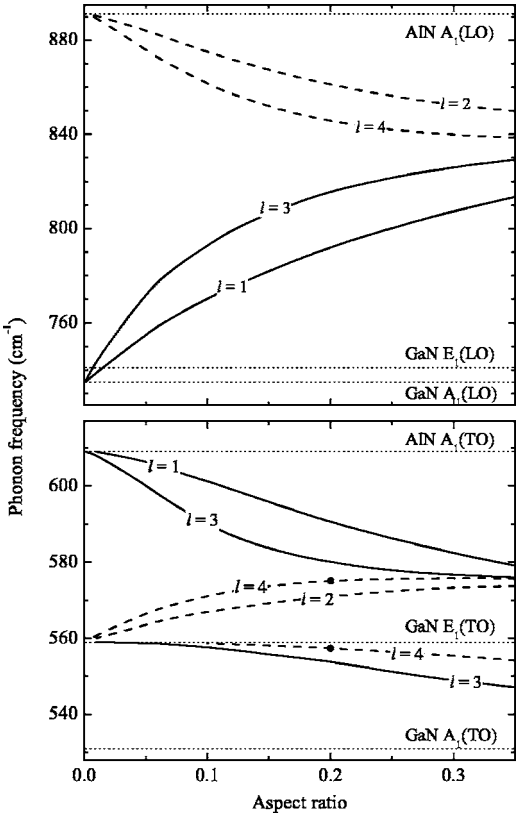

FIG. 5. Frequencies of the polar optical phonons with $m=0$ for an oblate spheroid GaN QD embedded in an AlN matrix as a function of the dot aspect ratio. For clarity, the frequencies of even and odd modes are plotted with dashed and solid lines, respectively. The full circles at $h/R=0.2$ correspond to the frequencies of the modes plotted in Fig. 6.

aspect ratio and the GaN or AlN character gets more mixed with increasing h/R, as can be observed in Fig. 5.

The potential corresponding to two different polar optical modes of a GaN/AlN QD with an aspect ratio of 0.2 is shown in Fig. 6. The chosen modes are marked with solid circles in Fig. 5. The upper plot corresponds to a TO quasiconfined mode and the lower one represents an interface optical mode. For the quasiconfined mode, Fig. 6(a), the potential varies faster inside the dot, going from negative to positive values when moving from the dot center toward the surfaces. As a result, the electric field $\mathbf{E}=-\boldsymbol{\nabla}V$ of the quasiconfined mode reaches its maximum value inside the QD. On the other hand, the maximum of $\mathbf{E}$ occurs closer to the dot surface for the interface mode, since the potential shown in Fig. 6(b) peaks at the dot surface and decays fast when moving away from it. In both cases the potential penetrates deeply into the AlN barrier.

B. Strain effects

We now turn our attention to the effect of strain on the Raman spectra of the QD's. Most previous Raman studies have been interpreted assuming the biaxial strain approximation for the GaN QD's,[6–8] so that

$$\varepsilon_{xx} = \varepsilon_{yy},$$

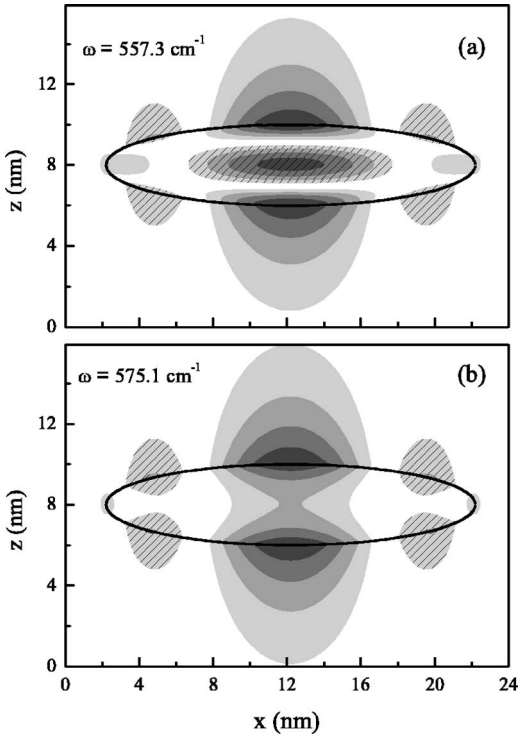

FIG. 6. Contour plots of the mode potential corresponding to two different modes with $m=0$ and $l=4$ of an oblate spheroid with an aspect ratio of 0.2. (a) corresponds to a quasiconfined TO mode, while (b) shows the potential of an interface mode. The white areas indicate that the potential is equal to zero, and the darker the solid (patterned) areas, the more positive (negative) the potential. The solid line represents the QD surface.

$$\varepsilon_{zz} = -\frac{2C_{13}}{C_{33}}\varepsilon_{xx} = -0.53\varepsilon_{xx}. \tag{10}$$

In this work, we have performed realistic calculations of the strain distribution in the QD multilayer system under study. The theoretical model employed is based on Eshelby's method of inclusions[25] as applied to hexagonal crystals by Andreev *et al.*[26] The only input parameters of the model are the lattice mismatch between the inclusion (GaN QD and WL) and the surrounding matrix (AlN barriers), defined as

$$\varepsilon_a = \frac{a_{\mathrm{AlN}}}{a_{\mathrm{GaN}}} - 1 = -2.4\,\%, \quad \varepsilon_c = \frac{c_{\mathrm{AlN}}}{c_{\mathrm{GaN}}} - 1 = -3.9\,\%, \tag{11}$$

and the elastic constants of both materials. For the sake of simplicity, the elastic constants are assumed to be the same (equal to those of the matrix) throughout the whole structure. This is a good approximation within the uncertainty of the elastic constant values.[27] In addition, taking into account the linearity of the elastic problem, the strain distribution of a QD array can be easily obtained as a superposition of the results for a single QD. Details about the theoretical model are reported elsewhere.[28]

This model has been used to calculate the strain distribution in a system containing 50 layers of GaN QD's standing

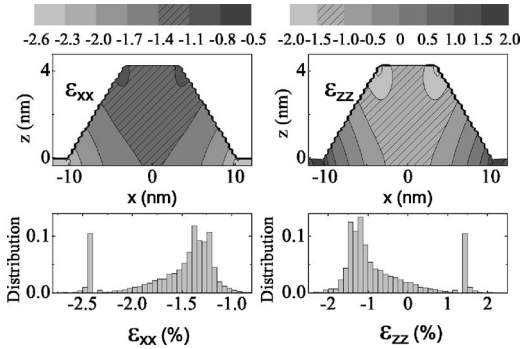

FIG. 7. Contour plots of the calculated strain components ε_{xx} and ε_{zz} in the GaN QD and WL. For clarity we have not drawn the QD's in scale. The histograms in the bottom part of the figure represent the number of pixels corresponding to a certain value of strain within the section of the quantum dot shown in the upper part of the figure. The distribution is normalized to the total number of pixels.

on a thin WL and embedded in an infinite AlN matrix. The dots are truncated cones of height and diameter as measured by HRTEM for sample *S*1. Figure 7 displays the cross section of the in-plane, ε_{xx}, and perpendicular, ε_{zz}, strain components corresponding to the QD and the WL in the central period of the multilayer. The strain distribution in the AlN spacers surrounding the QD's is plotted in Fig. 8. We checked that the central period is representative of most of the sample and that only the last three periods at the bottom and top of the stack show slightly different strain distributions. The strain ε_{xx} is obtained by an in-plane angular average. As shown in Fig. 7, ε_{xx} inside the dot becomes less negative than in the WL, −2.4%, as a result of the partial in-plane relaxation taking place inside the dots. The deviation from the WL biaxial strain is more pronounced for ε_{zz}, which changes from being tensile in the WL (+1.4%) to being compressive (∼−2%) at the top of the dot. As can be deduced from the histograms of Fig. 7, the mean strain component values in the QD volume are $\langle\varepsilon_{xx}\rangle=-1.3\pm0.2$ % and $\langle\varepsilon_{zz}\rangle=-1.0\pm0.3$ %, and their ratio $\langle\varepsilon_{zz}\rangle/\langle\varepsilon_{xx}\rangle=+0.8$ is clearly away from the biaxial value of Eq. (10). The most strained regions of the AlN spacers (see Fig. 8) are those between the vertically aligned dots, with mean values $\langle\varepsilon_{xx}\rangle=0.2\%$ and $\langle\varepsilon_{zz}\rangle=-0.5\%$.

In a bulk semiconductor, the frequency shift, $\Delta\omega=\omega-\omega_0$, with respect to the unstrained mode frequency, ω_0 (see Table I), of the different Raman modes can be written in terms of ε_{xx} and ε_{zz} as[29]

$$\Delta\omega_\lambda = 2a_\lambda\varepsilon_{xx} + b_\lambda\varepsilon_{zz}, \tag{12}$$

where a_λ and b_λ are the phonon deformation potentials. Equation (12) is valid for strain fields isotropic on the *xy* plane ($\varepsilon_{xx}=\varepsilon_{yy}$) and with vanishing shear components ($\varepsilon_{ij}=0, i\neq j$).[29] These conditions are satisfied by the angular average strain of pyramidal dots. In order to quantify the effect of strain on the frequencies of the QD vibrational modes, one can consider that the atoms in a dot vibrate in the same manner as in a bulk sample but under the influence of an average strain field. The values of $\Delta\omega_\lambda$ for the different GaN Raman modes calculated following Eq. (12) are summarized in Table II. The frequency shift of E_1(LO) has not been calculated because its phonon deformation potentials have not been reported in the literature yet. The frequency shifts of the AlN modes have also been calculated following Eq. (12) with the experimental values for a_λ and b_λ reported in Ref. 32. In this case, $\Delta\omega_\lambda$ are very small and within the calculated error bars since the frequency shifts due to $\langle\varepsilon_{xx}\rangle$ and $\langle\varepsilon_{zz}\rangle$ for AlN compensate each other.

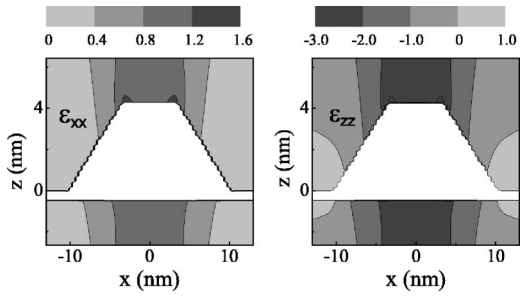

FIG. 8. Contour plots of the calculated strain components ε_{xx} and ε_{zz} in the AlN barrier.

TABLE II. Calculated strain-induced shifts of the GaN Raman frequencies. The phonon deformation potential constants a_λ and b_λ are given in the last two rows. All values are given in cm^{-1}.

	E_{2H}	A_1(TO)	E_1(TO)	A_1(LO)
$\Delta\omega_\lambda$	34±6	31±8	30±4	30±6
a_λ	−850±30[a]	−630±40[a]	−820±25[a]	−685±40[b]
b_λ	−920±60[a]	−1290±80[a]	−680±50[a]	−997±70[b]

[a]Value taken from Ref. 31.
[b]Value taken from Ref. 30.

C. Comparison with the experimental results

Let us reexamine now the Raman spectra of sample *S*1 shown in Fig. 2 in the light of the theoretical results exposed in the previous sections. First, we discuss the observed frequency shift of the E_{2H} mode (36±2 cm^{-1}). Taking into account the nonpolar nature of this mode and its flat frequency dispersion along the [0001] direction, confinement effects only introduce a marginal frequency shift of less than 1 cm^{-1}. Thus, the observed $\Delta\omega$ can be attributed to the effects of the strain field. Indeed, the calculated $\Delta\omega$ for the E_{2H} mode (see Table II) is in excellent agreement with the experimental results.

The analysis of the polar modes, *A*, *B*, *C*, and *D* is more complicated since these are strongly affected by the presence of interfaces as well as by the strain field of the dot system. In order to estimate the influence of the QD confinement, the dot can be approximated by an oblate GaN spheroid of $h/R\approx0.2$ (the aspect ratio of sample *S*1 is 0.21, as determined by HRTEM) embedded in an infinite AlN matrix. Although this is only a coarse approximation of the dot shape, it can provide valuable qualitative information about the confinement effects on the optical polar modes. In spite of the

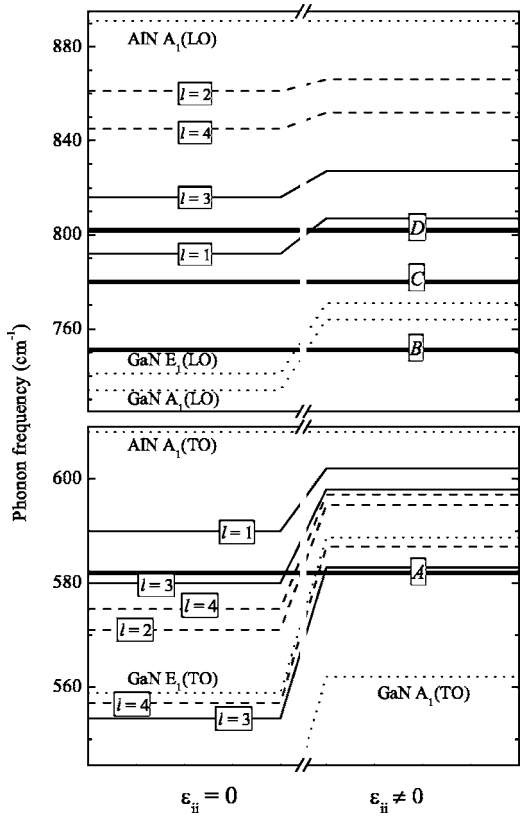

FIG. 9. Calculated frequencies of the polar TO (bottom figure) and LO (top figure) modes of an oblate GaN/AlN QD with $h/R=0.2$ with ($\varepsilon_{ii}\neq 0$) and without ($\varepsilon_{ii}=0$) taking the strain state of the dot into account. The experimental frequencies of modes *A*, *B*, *C*, and *D* of sample *S*1 are shown as solid thick lines. The dotted lines represent the bulk GaN and AlN frequencies.

penetration of the polar modes into the barrier shown in Fig. 6, vibrational coupling between different QD layers can be neglected for the 8.6 nm AlN spacer of sample *S*1. The frequencies of the modes for an unstrained GaN/AlN spheroid QD already calculated in Sec. IV B are shown on the left hand side of Fig. 9 together with the experimental frequencies of modes *A*, *B*, *C*, and *D*.

The highest-symmetry TO modes are the $l=3$ quasiconfined mode and the $l=1,2$ interface modes. The three of them lie close to the experimental *A* peak (see Fig. 9). Out of the four LO interface modes found at higher frequencies, those with $l=1$ and 3 are in reasonable agreement with peaks *C* and *D* in the spectra of sample *S*1.

In the previous discussion, the GaN/AlN QD has been considered fully relaxed and the unstrained values of the bulk phonon frequencies have been used in the calculations. This is far from reality, though, as already discussed in Sec. IV B. However, the average strain field approximation of Eq. (12) works well for the strain-induced Raman frequency shift of the nonpolar E_{2H} mode but is not appropriate for polar optical phonons. As shown in Fig. 6, both confined and interface polar modes penetrate deeply into the AlN barrier and it is expected that their frequencies are also influenced by the strain state of the barrier material, which is, generally, quite different from that of the GaN dot. In particular, the AlN matrix surrounding the dots in sample *S*1 (see Figs. 7 and 8) is much less strained than the QD's and its average phonon frequencies are those of bulk AlN. Therefore the strain-induced frequency shifts of the polar modes have been estimated following a different approach which combines strain and confinement effects: the anisotropic dielectric continuum model described in Sec. IV A has been applied to the case of a strained GaN QD embedded in an unstrained AlN matrix. The GaN dots are considered to be uniformly strained and their phonon frequencies are the bulk frequencies of Table I corrected by the calculated strain-induced $\Delta\omega$ of Table II. As mentioned before, the strain-induced shift of mode $E_1(\mathrm{LO})$ could not be calculated but we can assume that it is approximately equal to the shift of the $A_1(\mathrm{LO})$ mode, in the same way that $\Delta\omega$ for $E_1(\mathrm{TO})$ and $A_1(\mathrm{TO})$ are equal within the experimental error.

The secular equation (9) has been solved again for an oblate spheroidal GaN/AlN QD of $h/R=0.2$ after modifying the dielectric functions (3) of the dot to account for its new phonon frequencies shifted by strain. The results obtained by this procedure are summarized in the right hand side of Fig. 9. The TO quasiconfined mode ($m=0$ and $l=3$) has a corrected frequency of 583 cm^{-1} (i.e., a strain-induced $\Delta\omega$ of +29 cm^{-1}). This mode is in excellent agreement with the observed *A* Raman peak. Four interface modes with $l=1,2,3,4$ have their frequencies comprised between 595 and 602 cm^{-1} and their strain-induced frequency shifts (varying from 12 to 24 cm^{-1}) are smaller than for the quasiconfined mode. These modes may not be observed experimentally because they coincide with the much more intense $A_1(\mathrm{TO})$ mode of the AlN barrier. The LO interface modes are also blueshifted between 4 and 12 cm^{-1} and they appear between 807 and 865 cm^{-1}. Let us remark that the modes regarded as quasi-AlN LO interface modes are less shifted by strain than those with quasi-GaN character. When compared with the experimental frequencies of interface modes *C* and *D*, we still find a qualitative agreement between theory and experiment. The theoretical values are slightly overestimated but are still comprised within the large linewidth of these modes. Such large broadening can be attributed to the inhomogeneous distribution of dot sizes and the theoretically predicted high dispersion of LO interface mode frequencies with h/R reflected in Fig. 5. Finally, peak *B* in the Raman spectra of Figs. 2 and 3 is quite far from the calculated frequencies of Fig. 9. This mode shows better agreement with those of a much flatter spheroidal QD (with aspect ratio below 0.05) as can be seen in Fig. 5. The dots in the studied samples formed on top of a flat WL and the bottom interface of the QD is much flatter than the upper interface, as shown in Fig. 1. Hence, a possible explanation of the origin of peak *B* is that it is associated with an interface mode localized at the bottom surface of the self-assembled QD.

V. CONCLUSIONS

The Raman spectra of self-assembled GaN/AlN quantum dots have been investigated for a wide range of excitation energies. One nonpolar mode with E_2 symmetry and four polar optical modes have been assigned to the quantum dots:

A is transversal and *B*, *C*, and *D* are longitudinal. The quantum dot E_{2H} mode frequency is in excellent agreement with the results of a theoretical model taking into account the inhomogeneous elastic strain relaxation inside quantum dots of realistic shape. Hence, this mode behaves in the same manner as in the bulk material and its blueshifted frequency is due to the high compression state of the dots. On the other hand, the interpretation of the polar optical modes is more complicated. These are sensitive to the presence of interfaces and their frequencies depend on the shape and aspect ratio of the dot surface. In addition, polar modes are affected by the strain state of both the GaN dot and the AlN barrier as they are not fully confined inside the quantum dots. A theoretical model combining strain and confinement effects on the basis of the anisotropic dielectric continuum approximation has been applied to a GaN/AlN spheroidal quantum dot and shows reasonable qualitative agreement with the experimental results. We can then conclude that the *A* transversal polar mode could be quasiconfined in the dot and the longitudinal modes are more likely to be localized at the interfaces. Modes *C* and *D* show good agreement with the higher aspect ratio of the dots and can be attributed to the upper surface, whereas mode *B* is assigned to the flat bottom surface of the dot. The theoretical model also predicts that the strain-induced frequency shift of different interface polar optical modes can be rather different depending on their AlN-like or GaN-like character.

ACKNOWLEDGMENTS

The authors are thankful to the Ministerio de Eduación y Ciencia (Grant No. MAT2003-00399), to Generalitat Valenciana, and to SANDiE European Network (Grant No. NMP4-CT-2004-500101) for financial support.

[1] B. Daudin, F. Widmann, G. Feuillet, Y. Samson, M. Arlery, and J. L. Rouvière, Phys. Rev. B **56**, R7069 (1997).
[2] S. De Rinaldis, I. D'Amico, E. Biolatti, R. Rinaldi, R. Cingolani, and F. Rossi, Phys. Rev. B **65**, 081309(R) (2002).
[3] F. Widmann, J. Simon, B. Daudin, G. Feuillet, J. L. Rouvière, N. T. Pelekanos, and G. Fishman, Phys. Rev. B **58**, R15989 (1998).
[4] F. Bernardini, V. Fiorentini, and D. Vanderbilt, Phys. Rev. B **56**, R10024 (1997).
[5] J. Stangl, V. Holý, and G. Bauer, Rev. Mod. Phys. **76**, 725 (2004).
[6] J. Gleize, F. Demangeot, J. Frandon, M. A. Renucci, C. Adelmann, B. Daudin, G. Feuillet, B. Damilano, N. Grandjean, and J. Massies, Appl. Phys. Lett. **77**, 2174 (2000).
[7] J. Gleize, F. Demangeot, J. Frandon, M. A. Renucci, M. Kuball, B. Damilano, N. Grandjean, and J. Massies, Appl. Phys. Lett. **79**, 686 (2001).
[8] M. Kuball, J. Gleize, S. Tanaka, and Y. Aoyagi, Appl. Phys. Lett. **78**, 987 (2001).
[9] A. Cros, N. Garro, J. M. Llorens, A. García-Cristóbal, A. Cantarero, N. Gogneau, E. Monroy, and B. Daudin, Phys. Rev. B **73**, 115313 (2006).
[10] S. M. Komirenko, K. W. Kim, M. A. Stroscio, and M. Dutta, Phys. Rev. B **59**, 5013 (1999).
[11] J. Gleize, M. A. Renucci, J. Frandon, and F. Demangeot, Phys. Rev. B **60**, 15985 (1999).
[12] D. A. Romanov, V. V. Mitin, and M. A. Stroscio, Phys. Rev. B **66**, 115321 (2002).
[13] V. A. Fonoberov and A. A. Balandin, Phys. Rev. B **70**, 233205 (2004); J. Phys.: Condens. Matter **17**, 1085 (2005).
[14] T. Shibata, K. Asai, T. Nagai, S. Sumiya, M. Tanaka, O. Oda, H. Miyake, and K. Hiramatsu, in *GaN and Related Alloys*, edited by J. E. Northrup, J. Neugebauer, D. C. Look, S. F. Chichibu, and H. Riechert, MRS Symposia Proceedings No. 693 (Materials Research Society, Pittsburgh, 2002), p. 541.
[15] N. Gogneau, D. Jalabert, E. Monroy, T. Shibata, M. Tanaka, and B. Daudin, J. Appl. Phys. **94**, 2254 (2003).
[16] V. Chamard, T. H. Metzger, M. Stucki, V. Holý, M. Tolan, E. Bellet-Amalric, C. Adelmann, B. Daudin, and H. Mariette, Europhys. Lett. **63**, 268 (2003).
[17] E. Sarigiannidou, E. Monroy, B. Daudin, J. L. Rouvière, and A. D. Andreev, Appl. Phys. Lett. **87**, 203112 (2005).
[18] N. Gogneau, F. Fossard, E. Monroy, S. Monnoye, H. Mank, and B. Daudin, Appl. Phys. Lett. **84**, 4224 (2004).
[19] F. Widmann, B. Daudin, G. Feuillet, Y. Samson, J. L. Rouvière, and N. T. Pelekanos, J. Appl. Phys. **83**, 7618 (1998).
[20] V. Y. Davydov, Y. E. Kitaev, I. N. Goncharuk, A. N. Smirnov, J. Graul, O. Semchinova, D. Uffmann, M. B. Smirnov, A. P. Mirgorodsky, and R. A. Evarestov, Phys. Rev. B **58**, 12899 (1998).
[21] A. R. Goñi, H. Siegle, K. Syassen, C. Thomsen, and J. M. Wagner, Phys. Rev. B **64**, 035205 (2001).
[22] M. Cardona, in *Light Scattering in Solids II*, edited by M. Cardona and G. Güntherodt (Springer, Berlin, 1982).
[23] J. Gleize, J. Frandon, M. A. Renucci, and F. Bechstedt, Phys. Rev. B **63**, 073308(R) (2001).
[24] P. A. Knipp and T. L. Reinecke, Phys. Rev. B **46**, 10310 (1992).
[25] J. D. Eshelby, Proc. R. Soc. London, Ser. A **241**, 376 (1957).
[26] A. D. Andreev and E. P. O'Reilly, Phys. Rev. B **62**, 15851 (2000).
[27] I. Vurgaftman and J. R. Meyer, J. Appl. Phys. **94**, 3675 (2003).
[28] A. García-Cristóbal and J. M. Llorens (unpublished).
[29] A. Anastassakis and M. Cardona, in *High Pressure in Semiconductor Physics II*, edited by T. Suski and W. Paul (Academic Press, San Diego, 1998).
[30] F. Demangeot, J. Frandon, M. A. Renucci, O. Briot, B. Gil, and R. L. Aulombard, Solid State Commun. **100**, 207 (1996).
[31] V. Y. Davydov, N. S. Averkiev, D. K. Nelson, I. P. Nikitina, A. S. Polkovnikov, A. N. Smirnov, M. A. Jacobson, and O. K. Semchinova, J. Appl. Phys. **82**, 5097 (1997).
[32] J. Gleize, M. A. Renucci, J. Frandon, E. Bellet-Amalric, and B. Daudin, J. Appl. Phys. **93**, 2065 (2003).